Using spin-polarized neutron reflectivity to probe mesoscopic vortex states in a Pb thin-film superconductor

A. J. Drew,[1,2] M. W. Wisemayer,[2] D. O. G. Heron,[2] S. Lister,[2] S. L. Lee,[2] A. Potenza,[3,4] C. H. Marrows,[3] R. M. Dalgliesh,[5] T. R. Charlton,[5] and S. Langridge[5]

[1]*Department of Physics, University of Fribourg, Fribourg CH-1700, Switzerland*

[2]*School of Physics and Astronomy, University of St. Andrews, St. Andrews, KY16 9SS Scotland, United Kingdom*

[3]*School of Physics and Astronomy, University of Leeds, Leeds LS2 9JT, United Kingdom*

[4]*Diamond Light Source Ltd., Harwell Science and Innovation Campus, Chilton, Didcot, Oxfordshire OX11 0DE, United Kingdom*

[5]*ISIS, Rutherford Appleton Laboratory, Harwell Science and Innovation Campus, Didcot, Oxfordshire OX11 0QX, United Kingdom*

(Received 3 September 2009; published 14 October 2009)

Spin-polarized neutron-reflectivity measurements have been performed on superconducting Pb films. For fields applied in the plane of the film we are able to determine the magnetic field profile across the thickness of the film in the superconducting state. This allows the direct observation of distinct mesoscopic ground states in this geometry, from Meissner expulsion to a double row of vortices, which occur as a function of film thickness and external magnetic field. The data can be compared directly with solutions of the time-dependent Ginzburg-Landau equations, where we demonstrate good agreement between data and simulation. This provides a powerful demonstration of this widely applicable experimental technique to study mesoscopic ground states and a useful validation of this theoretical approach.

DOI: 10.1103/PhysRevB.80.134510 PACS number(s): 74.78.Db, 74.20.De, 74.25.Op

I. INTRODUCTION

The behavior of magnetic-flux vortices, which form in the mixed state of type II superconductors, is a subject which commands significant attention in the literature. Vortices formed in bulk superconductors have become a testing ground for theoretical studies examining the statistical physics and classical correlations associated with disordered systems.[1] There is also increasing interest in the behavior of superconducting thin-film structures, particularly in combination with other materials such as ferromagnetic layers.[2–5] In thin-film structures where vortices are present it is important that the mesoscopic states of such systems are well understood.[2] Many techniques used to examine the spatial configuration of vortices only image vortices at their point of exit through the surface.[6–8] Bulk probes such as small-angle neutron diffraction[9,10] and muon-spin rotation[11,12] require large volumes of sample so are not generally suitable for thin films. The recently developed low-energy muon technique[13] has been used successfully to determine the magnetic and superconducting properties of thin films.[2,14,15] However, at present this technique is limited to low values of applied field.[13]

In addition to inter-vortex interactions and defect pinning, vortices are also are influenced by surface effects.[16] When a magnetic field is applied *parallel* to the surface of a thin film, having a thickness comparable to the London penetration depth, the surface interaction with the vortices is particularly strong. When this is the case, one would expect surface-induced ordering of the vortices[17] with different numbers of vortex rows depending on the applied magnetic field and relative thickness of the film. Similar effects have been observed in mesoscopic quantum dots probed using ballistic Hall magnetometry.[18] Results to date mainly derive from macroscopic probes such as magnetization, electron tunneling, and resistivity.[19] However, these techniques only measure average magnetization or effects of vortex motion and it is therefore difficult to obtain direct information on the *microscopic* arrangement of the vortices.

Specular spin-polarized neutron reflectivity (SPNR) is sensitive to the spatial variation in magnetic flux across the thickness of a thin-film sample and has been used to study the superconducting state in a number of systems. As with the experiments presented in this paper, many of these have been carried out with the field applied parallel to the surface of the films. The technique was first used by Felcher *et al.*[20] on relatively thick films of Nb (5 μm), where the flux variation due to Meissner expulsion was measured at one surface. This allowed the superconducting penetration depth λ to be determined. A similar approach was used by Nutley *et al.*[21] on a thick Pb film to study the surface superconductivity and to look for nonlocal effects, although the experiment proved insufficiently sensitive to observe the latter. Experiments on thinner films of Nb grown on Si were carried out by Zhang *et al.*[22] in which neutrons were incident on either the vacuum or the Si side of the sample, the latter being found to yield higher-quality data. More significantly the thinnest sample investigated (300 nm) was of sufficient quality that strong interference fringes could be observed that allowed a precise fit to a simple London model of Meissner expulsion below the lower critical field H_{c_1}. Han *et al.*[23] performed SPNR measurements on a 600-nm-thick film of the cuprate material $YBa_2CaCu_3O_{7-x}$, which as an extreme type II material ($\lambda \gg \xi$, where ξ is the superconducting coherence length) that should be well described by the London model. To fit the data they developed a model in the London limit in which vortices were present in the sample, giving contributions to the flux profile across the sample additional to those produced by surface screening. In the analysis of the data they assumed that vortices were *uniformly distributed* across the width of the sample since the data were inconsistent with a strong localization of the vortices in the center of the film.

They also presented simulations which indicated that, in principle, the technique could discriminate between a single row or double row of vortices localized on planes at the center of the film, or a localized band of vortices disordered over a Gaussian distribution about the center of the film. However, the distinguishing signatures occurred at scattering vectors higher than those that could be obtained in those experiments, so the main conclusion of that paper was that SPNR is able to detect the presence of vortices within a film in a parallel field geometry. Due to the small coherence length of the cuprates these systems are highly susceptible to point pinning by defects and indeed significant hysteresis was observed in those experiments. Together with the relatively large sample thickness ($\sim 4\lambda$), this probably also explained the uniform distribution of vortices across the sample. The average vortex density was also an empirically determined parameter in those experiments. Thus this experiment on the cuprate material by Han *et al.*[23] was not able to observe distinct equilibrium mesoscopic states. It is the latter that is subject of the present work.

In this paper we present work on a conventional superconductor, Pb, which has a $\xi \sim \lambda \sim d$, where d is the thickness of the superconducting layer. This requires a much more general and widely applicable description than the London model that makes no assumption about the vortex arrangement, for which we have adopted a time-dependent Ginzburg-Landau (TDGL) approach.[24] In comparison to cuprate materials, the Pb system carries the advantage that the normal-state cores of the vortices, of spatial extent ξ, have a much more significant influence on both the vortex arrangement and the reflectivity signal and hence allows a more precise determination of the mesoscopic state. The large value of ξ also means that defect pinning is much less significant than surface effects in controlling the vortex arrangement, which coupled with the small sample thicknesses chosen leads to the occurrence of distinct mesoscopic ground states that may be distinguished over the accessible range of scattering wavevectors. The good agreement between the TDGL model, which for the vortex states is not fitted but simply *simulated* based on independent measurements of ξ and λ, provides a powerful validation of this theoretical description of the vortex state. Moreover it also demonstrates that this combined theoretical and experimental approach can be extended to a range of materials in thin-film structures where the vortex state may be less well understood.[2]

II. EXPERIMENT

We performed the SPNR experiments using the CRISP reflectometer at ISIS, U.K. Measurements were carried out on three 20×22 mm Pb films of thickness 130, 195, and 250 nm, with an 8 nm Mo capping layer to inhibit oxidation. The thickness of the Pb films was varied in order to allow different regimes to be probed. The films were grown on silicon wafer (100) substrates using dc sputtering. The native oxide of the wafer was left intact, giving a growth surface for the Pb that was both flat and amorphous. The (100) orientation of the underlying Si lattice was thus irrelevant to the growth mode of the Pb. Also grown under exactly the same conditions in the same batch were smaller 12×4 mm samples for magnetization measurements. These films were characterized using *ex situ* x-ray reflectometry, dc-resistivity and magnetization measurements, and had a superconducting transition temperature of $T_c = 6.7$, 6.9, and 7.1 K for the 130-, 195-, and 250-nm-thick film, respectively. In order to model the reflectivity, we used an optical neutron-reflectivity model[25] with a realistic approximation for roughness.[26] For all experiments described the field was applied in the plane of the superconducting film.

To model the superconductivity we used a Ginzburg Landau (GL) approach, following the numerical method reported by Bolech *et al.*[24] In order to determine the order parameter ψ and vector potential $\boldsymbol{A}$ it is necessary to solve the TDGL equations

$$\frac{\partial \psi}{\partial t} = \frac{-1}{\eta}[(-i\nabla - \boldsymbol{A})^2 \psi + (1-T)(|\psi|^2 - 1)\psi] + f \qquad (1)$$

and

$$\frac{\partial \boldsymbol{A}}{\partial t} = (1-T)\Re[\psi^*(-\nabla - \boldsymbol{A})\psi] - \kappa^2 \nabla \times \nabla \times \boldsymbol{A}. \qquad (2)$$

Lengths have been scaled in units of $\xi(0)$, time in units of $\pi\hbar/(96K_B T_c)$, $\boldsymbol{A}$ in units of $H_{c_2}(0)\xi(0)$, temperature in units of T_c, and η is the ratio of the characteristic times for ψ and $\boldsymbol{A}$. Finally, f is a random thermal fluctuation with zero mean and a standard deviation of $\sigma = \sqrt{(\pi E_0 \Delta t/6)(T/T_c)}$, where Δt is the time step.

The numerical approximation used was a finite difference method.[27–30] The computational domain was a two-dimensional (2D) layer of thickness $d\xi(0)$ and length $250\xi(0)$ with d chosen in accordance with the experimental film thickness. The domain was divided into cells with an edge $0.25\xi(0)$ and at the boundaries $y = \pm(d/2)\xi(0)$, the y component of the current is set to zero. Periodic boundary conditions were imposed at $x = \pm 125\xi(0)$ to approximate an infinite film. The solution was obtained by fixing the temperature, GL parameter κ and the external field, H_a, at particular values (determined independently via experiment, see Sec. III), calculating the free energy every Δt and waiting until a stable solution was calculated. The criterion used to stop the solution was that the free energy must be constant to within 1 in 10^7 between time steps. The model does not include defect pinning justified both by the large coherence length and by the extremely close agreement between simulation and measurement. Hence the final result from the TDGL simulation is unaffected by the sample's history if given sufficient time.

III. RESULTS AND DISCUSSION

In Fig. 1 we plot the estimate of the superconducting upper critical field (H_{c_2}) as a function of temperature for two film thicknesses derived from superconducting quantum interference device measurements on the magnetization samples. We note that (as indicated by the solid fitted lines) close to T_c, the temperature dependence of H_{c_2} for the thinnest 130 nm film is of the form expected for 2D supercon-

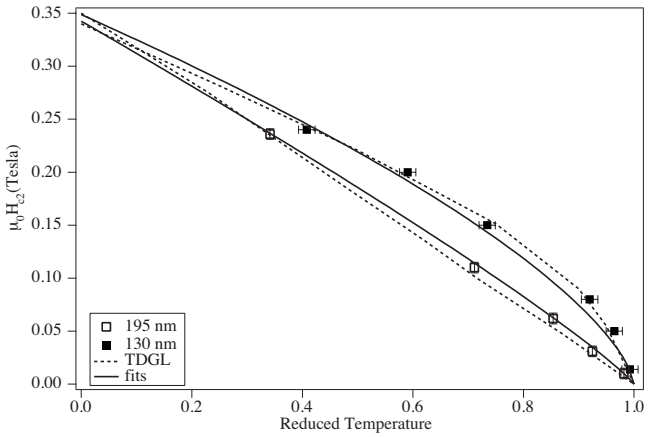

FIG. 1. The temperature dependence of the upper critical field $H_{c_2}(T)$ obtained from magnetization data for films of thickness 130 and 195 nm. Solid lines: simple analytical expressions consistent with the occurrence of 2D and 3D superconductivity, respectively (see text). Dashed lines: $H_{c_2}(T)$ calculated by numerical solution of our TDGL model (see text).

ducting behavior (thin-film limit) $[H_{c_2} \propto (T_c - T)^{1/2}]$, while the intermediate 195 nm film appears to correspond to three-dimensional (3D) behavior $[H_{c_2} \propto (T_c - T)]$.[31,32] Performing an extrapolation on the simple analytic fit to the data shown in Fig. 1, $B_{c_2}(0) = \mu_o H_{c_2}(0)$ is estimated to be 0.35 and 0.34 T for the 130 and 195 nm film, respectively, corresponding to a superconducting coherence length $\xi(0) \approx 31(1)$ nm. We will make use of these values in the simulations of the SPNR data which follow. Also shown are the $H_{c_2}(T)$ lines obtained from numerical solution of the TDGL Eqs. (1) and (2) using this value of $\xi(0)$ and the value of $\lambda(0)$ used below to model the neutron data of Fig. 2. The crossover with increasing film thickness from 2D to 3D superconductivity is a well-documented phenomenon in thin film and multilayered superconducting systems, e.g. (Refs. 31 and 32). Nonetheless, the TDGL curves, which are simulations and not fits, are in excellent agreement with both the measured values of $H_{c_2}(T)$ and with the simple analytical models also shown. This furthermore illustrates that the TDGL model we use is able to describe self-consistently both the macroscopic data and the SPNR data presented below using the same parameters.

In Fig. 2 we plot the SPNR data obtained from the 130 nm film, cooled in an applied field of 0.1 T to a temperature of 2.5 K. In a given layer α the neutron's potential energy has both a nuclear and a magnetic contribution such that $V_\alpha = (\hbar^2/2\pi m_n)\rho_\alpha b_\alpha - \boldsymbol{\mu}_n \cdot \boldsymbol{B}_\alpha$, where $\boldsymbol{\mu}_n$, b_α, $\boldsymbol{B}_\alpha$, and ρ_α are the neutron moment, the coherent nuclear scattering length, the magnetic-flux density (due to the external applied field $\boldsymbol{H}_e$ and sample magnetization), and the atomic density. The spin-dependent neutron signal arising from superconductivity was modeled using a spatially varying $\boldsymbol{B}_\alpha(y) = B_\alpha(y)\hat{z}$ calculated using the TDGL equations and also by a simple Meissner model [Eq. (3)] where appropriate. When using *spin-polarized* neutrons it is essential to fit simultaneously the *reflectivity* data in each spin channel containing both magnetic and nuclear contributions. Although the derived quantity $S_{\uparrow\downarrow} = (R_\uparrow - R_\downarrow)/(R_\uparrow + R_\downarrow)$, the spin asymmetry, provides a more intuitive and informative way to represent the data, it is not possible to separate the magnetic scattering from the nuclear scattering by fitting this quantity alone. Furthermore, fitting only $S_{\uparrow\downarrow}$ may also lead to systematic errors in the case where a significant background exists in the measured reflectivity.

In the Meissner state, for an external magnetic field applied parallel to the surface of the film (with a magnitude lower than the lower superconducting critical field H_{c_1}), the flux density will penetrate from both sides into a film of thickness d with a decreasing amplitude given in the London limit by

$$\boldsymbol{B}(y) = \mu_0 \boldsymbol{H}_e \frac{\cosh\left(\frac{2y-d}{2\lambda}\right)}{\cosh\left(\frac{d}{2\lambda}\right)}. \quad (3)$$

This was found to give a good description of the data for the 130 nm film (Fig. 2), from which the penetration depth λ was determined to be 78(3) nm. For this film no evidence for vortex nucleation was found at any field measured, up to a maximum value of 0.2 T, with the data at all fields being well described by Eq. (3). For completeness we have also used the more accurate TDGL approach to calculate the reflectivity curves for the 130 nm film using the same value of $\lambda = 78$ nm and using $\xi(0) = 31$ nm obtained from $H_{c_2}(T)$. This is shown in Fig. 2 to be consistent with the London-type Meissner state.

For clarity we emphasize at this point that in terms of the superconducting parameters $\xi(0)$ and $\lambda(0)$ we perform only two *fits* in this paper. First, the value of λ was extracted from the fit of the London model to the SPNR data for the Meissner expulsion state in the 130 nm film, as discussed above. Second the value of ξ was determined from the analytical expressions for $H_{c_2}(T)$ for samples in both the 2D and 3D superconducting regions, that is, the 130- and 195-nm-thick films, respectively (see Fig. 1). However, using these two values, $\lambda(0) = 78(3)$ nm and $\xi(0) = 31(1)$ nm, we have shown that the TDGL solutions also produce good descriptions of both the SPNR Meissner data (Fig. 2) and the upper critical field data (Fig. 1). For the data presented in the rest of this paper the London model provides an inappropriate description, so we use solutions of the TDGL equations. Moreover, we show that using just the above values of $\xi(0)$ and $\lambda(0)$, together with the measured value of the external field, we can produce curves corresponding to distinct mesoscopic vortex states that are in good agreement with the measured SPNR spin asymmetry. We further stress that these are not fits but simulated predictions of these equilibrium mesoscopic states that emerge naturally from the solutions of the TDGL for these parameters. The only fitted parameters in each case are the sample thickness.

Although very pure Pb is a type I superconductor, these sputtered samples have a Ginzburg-Landau parameter $\kappa \approx 2.5$, so are type II and can contain vortices. Figure 3 shows the measured spin asymmetry of the thicker films and a calculation based on our TDGL solution. The samples were cooled in an applied field of 50 mT and 0.1 T for the 195 nm

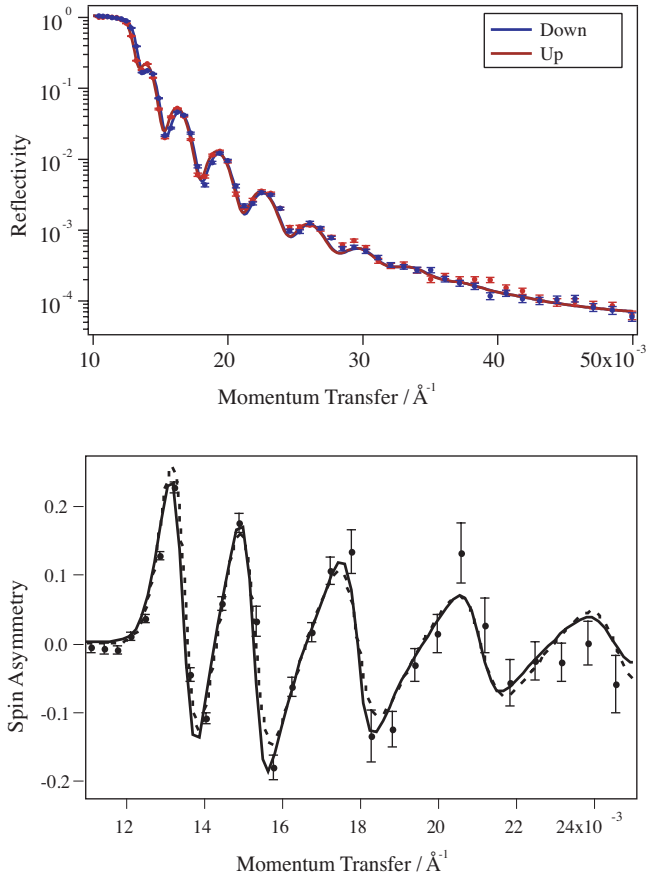

FIG. 2. (Color) Top: spin-dependent reflectivity data from our thinnest sample, 130 nm, measured at an applied field of 0.1 T. The data has been fitted using a simple Meissner model in the London limit. Bottom: a more transparent way of representing the purely magnetic scattering is to plot the spin asymmetry $S_{\uparrow\downarrow}$ (see text). Solid line: fit to Eq. (3). Dashed line: a solution of the TDGL Eqs. (1) and (2) using the values for λ, d obtained from the London model fits. The values of the reduced temperature t, H_{c_2}, and hence ξ and $\kappa=\lambda/\xi=2.5$, are derived from the magnetization data of Fig. 1 (see text). The TDGL simulations use a value $d=4.75\xi(0)$.

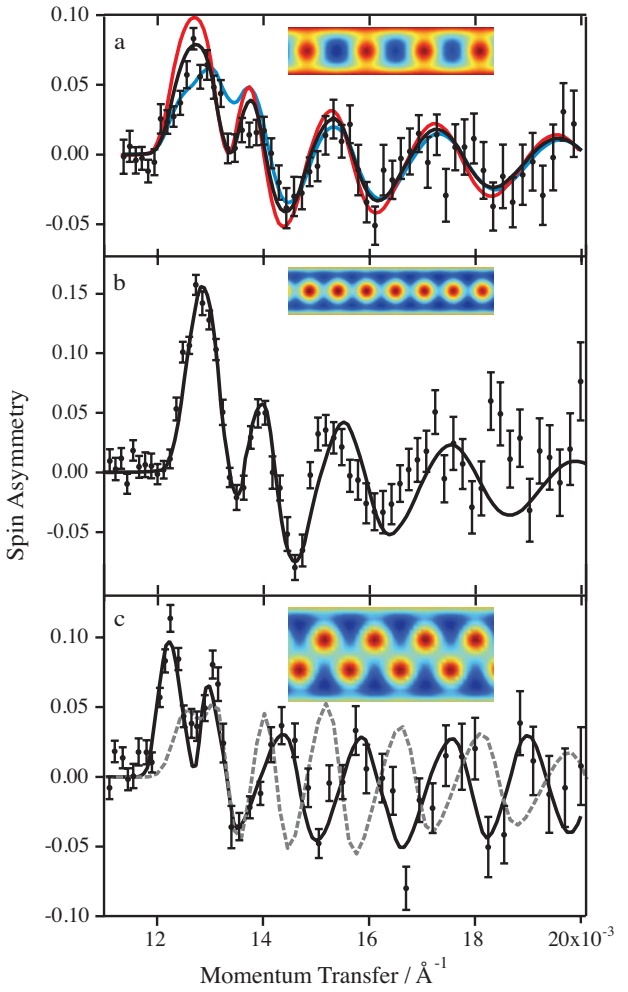

FIG. 3. (Color) Spin asymmetry $S_{\uparrow\downarrow}$ for (a) 195 nm film in 50 mT. (b) 195 nm film in 100 mT. (c) 250 nm film in 50 mT. The insets show color image plots of the magnetic-flux density corresponding to the equilibrium numerical solutions of the TDGL Eqs. (1) and (2) at the fields applied in the experiment. The solid black lines are the $S_{\uparrow\downarrow}$ curves that correspond to these solutions. Only after individual spin channel analysis was satisfactorily completed was $S_{\uparrow\downarrow}$ constructed. We note that layer thicknesses d were fitted but all other quantities were obtained independently. The blue and red curves in (a) are solutions to the TDGL equations for applied fields above and below that applied in the experiment (56 and 44 mT, respectively). The dashed line in (c) is a simulation using a London model for a single row of vortices having similar flux density to the TDGL solution (see text).

film and 50 mT for the 250 nm film, to a temperature of 2.5 K. For these solutions, we used $\kappa=2.5$ which is consistent with the estimate of $\xi(0)$ from the magnetization measurements (Fig. 1) and $\lambda=78$ nm from the 130 nm film SPNR results (Fig. 2). The thickness d, chosen in accordance with the film thickness found by fitting the nuclear part of the SPNR data was kept fixed at $6.25\xi(0)$ and $8\xi(0)$ for the 195 and 250 nm films, respectively. The reduced temperature t and H_{c_2} were also kept fixed at the experimentally measured quantities. The agreement between the model and the data is remarkably good, especially considering that these simulations are based entirely on *independently* determined parameters.

In both experiment and simulation the Meissner state of the 130 nm film persists to applied fields higher than those available on the experiment. In contrast for the thicker 195 nm film, a single row of vortices is observed along the center of the film [Figs. 3(a) and 3(b)]. In order to give an indication of the degree of quantitative agreement between the TDGL solutions and the data we also include in Fig. 3(a) two additional spin asymmetry curves corresponding to different lineal densities of vortices within the row, which we achieved by forcing the external applied field in the simulations to differ from those in the experiment. The fields were chosen to give lineal density variations of $\pm 12\%$ which show disagreement with the data mainly at low q, understandable since these correspond simply to flux density variations. We note however that at higher q the curves are rather similar since these q values are more sensitive to changes in the *arrangement* of the vortices as manifest in the flux profile across the width of the sample (see, e.g., Ref. 23). It is reassuring however that for a given applied field the

TDGL solutions produce good agreement over the whole q range for both the arrangement (a single row) and the average internal lineal flux density.

As the field is increased, as shown for example in Fig. 3(b), the concentration of vortices increases, as expected. In the equilibrium state the vortices nonetheless remain confined to the center of the film, although in the simulations they are nucleated at the surface of the film and migrate to the center. One can understand this heuristically by noting that for the case of a single vortex an effective repulsion exists between the surface and the vortex. For the case of multiple vortices one must also consider the mutual repulsion between vortices. In this film, at the fields measured the vortex density is such that repulsion from the surface is dominant over the inter-vortex interaction, confining all vortices to the center of the film. In the thicker film [Fig. 3(c)], on the other hand, where $d \sim 3.5\lambda$, we observe a double layer of vortices in the film. Here the vortices are able to move further from the center of the film, thus enabling a reduction in the interaction energy between the vortices as they move further apart. A zigzag structure is therefore formed along the center of the film.

To further illustrate the quality of agreement between the data and the TDGL model, we also include in the Fig. 3(c) the simulated signal that would arise from a *single* row of London vortices constrained to lie at the center of the film and having a similar flux density. We have chosen to use a London model for this comparison since we are then able to arbitrarily assign an internal flux density and vortex arrangement [one-dimensional (1D) lattice] to compare with the 2D (zigzag) arrangement predicted by the TDGL model. No such comparison is possible using only the TDGL since the solution is unphysical; both the internal flux density and vortex positions naturally arise from a minimization of the free energy for a given external field and sample thickness. Nonetheless, the comparison is useful in that it illustrates that the information allowing 1D and 2D lattice structures to be distinguished comes from higher momentum transfer values in the SPNR data. This fact was also noted by Han *et al.*[23] who simulated various vortex arrangements using a constrained London model but were unable to obtain useful SPNR data beyond the first peak in the spin asymmetry plots. Thus experimentally, unlike the present case, they were unable to observe the transition between these distinct mesoscopic states. Moreover, most likely due to the existence of strong defect pinning in their cuprate samples, their results even over the observable q range were found to be most consistent with a uniform distribution of vortices throughout the thickness of the sample and therefore could not be identified with well-defined mesoscopic states.

A transition with increasing field from a 1D to a 2D row of vortices was also predicted by Guimpel *et al.*,[19] using Tinkham's formalism to calculate the Gibbs free energy.[31] They performed experiments on Nb/Cu multilayers, assuming a state of isotropic and homogeneous superconductivity due to the strong interlayer coupling across the Cu layers via the proximity effect. The flux expulsion from the sample was measured as a function of applied field and the results compared to the simulations which showed similar features and trends, including maxima in the field-dependent data at the boundaries between the Meissner to 1D region and between the 1D and 2D region. While the features measured and the order of magnitude of flux expulsion agreed with data, the agreement between experiment and the simple model used was only qualitative. We contrast that work with our current results, where we use the TDGL approach not only to achieve a *quantitative* agreement with the average flux density inside the sample, but where we are also able to describe accurately the *spatial variation* in the flux density across the sample as measured by SPNR. Furthermore, the measured changes in this spatial variation with field are in agreement with the 1D to 2D transition predicted by TDGL without using any adjustable parameters.

IV. CONCLUSION

We have used SPNR to investigate the changes in the flux density profile across the thickness of a thin-film superconductor with the field directed parallel to the plane of the film. By careful choice of sample thickness relative to characteristic superconducting length scales and applied field we have measured the SPNR spin asymmetry over a sufficient momentum transfer range to allow us to clearly distinguish between different mesoscopic ground states. These are: a Meissner state; a 1D vortex lattice state in which the vortices are confined to a plane at the center of the film and a 2D vortex lattice state in which vortices are confined to two parallel planes close to the center of the sample (Fig. 3). As in previous work[20–23] the penetration depth was extracted from the SPNR data in the Meissner state using a simple London model and the coherence length was determined from magnetization measurement using the well-known Tinkham expressions for the upper critical field.[31,32] However, by solving the TDGL equations for all external fields measured we have furthermore been able to produce good quantitative descriptions of the SPNR spectra without any further adjustable parameters. This TDGL formalism can also be used to self-consistently describe the bulk $H_{c_2}(T)$ measurements and the SPNR measurements of the Meissner state.

We have thus demonstrated that the spatially sensitive SPNR technique is able to distinguish between different mesoscopic ground states well beyond any previous application of this approach in thin-film superconductors in this geometry. Moreover the good agreement between the solutions of the TDGL and all of our data not only provides an elegant verification of the validity of the TDGL model used but provides a powerful tool with which to detect deviations from this model which may occur in more exotic superconducting systems.

ACKNOWLEDGMENTS

This work was performed at ISIS, Rutherford Appleton Laboratory, Oxfordshire, U.K. We acknowledge financial support from the EPSRC (Grant Reference No. GR/N31382/01) and the European Commission (through Framework 6 project SFINx, under Grant No. NMP2-CT-2003-505587).

[1] G. Blatter, M. V. Feigel'man, V. B. Geshkenbein, A. I. Larkin, and V. M. Vinokur, Rev. Mod. Phys. **66**, 1125 (1994).
[2] A. Drew, S. L. Lee1, D. Charalambous, A. Potenza, C. Marrows, H. Luetkens, A. Suter, T. Prokscha, R. Khasanov, E. Morenzoni, D. Ucko, and E. M. Forgan, Phys. Rev. Lett. **95**, 197201 (2005).
[3] T. Kontos, M. Aprili, J. Lesueur, F. Genêt, B. Stephanidis, and R. Boursier, Phys. Rev. Lett. **89**, 137007 (2002).
[4] A. Yu. Rusanov, S. Habraken, and J. Aarts, Phys. Rev. B **73**, 060505(R) (2006).
[5] A. Potenza and C. H. Marrows, Phys. Rev. B **71**, 180503(R) (2005).
[6] P. L. Gammel, D. J. Bishop, G. J. Dolan, J. R. Kwo, C. A. Murray, L. F. Schneemeyer, and J. V. Waszczak, Phys. Rev. Lett. **59**, 2592 (1987).
[7] K. Harada, T. Matsuda, J. Bonevich, M. Igarashi, S. Kondo, G. Pozzi, U. Kawabe, and A. Tonomura, Nature (London) **360**, 51 (1992).
[8] J. E. Bonevich, K. Harada, T. Matsuda, H. Kasai, T. Yoshida, G. Pozzi, and A. Tonomura, Phys. Rev. Lett. **70**, 2952 (1993).
[9] R. Gilardi, J. Mesot, A. Drew, U. Divakar, S. L. Lee, E. M. Forgan, O. Zaharko, K. Conder, V. K. Aswal, C. D. Dewhurst, R. Cubitt, N. Momono, and M. Oda, Phys. Rev. Lett. **88**, 217003 (2002).
[10] E. M. Forgan, S. J. Levett, P. G. Kealey, R. Cubitt, C. D. Dewhurst, and D. Fort, Phys. Rev. Lett. **88**, 167003 (2002).
[11] U. Divakar, A. J. Drew, S. L. Lee1, R. Gilardi, J. Mesot, F. Y. Ogrin, D. Charalambous, E. M. Forgan, G. I. Menon, N. Momono, M. Oda, C. D. Dewhurst, and C. Baines, Phys. Rev. Lett. **92**, 237004 (2004).
[12] A. J. Drew, D. O. G. Heron, U. K. Divakar, S. L. Lee, R. Gilardi, J. Mesot, F. Y. Ogrin, D. Charalambous, N. Momono, M. Oda, and C. Baines, Physica B (Amsterdam) **374-375**, 203 (2006).
[13] T. Prokscha, E. Morenzoni, K. Deiters, F. Foroughi, D. George, R. Kobler, A. Suter, and V. Vrankovi, Physica B (Amsterdam) **374-375**, 460 (2006).
[14] H. Luetkens, J. Korecki, E. Morenzoni, T. Prokscha, M. Birke, H. Glückler, R. Khasanov, H.-H. Klauss, T. Ślezak, A. Suter, E. M. Forgan, Ch. Niedermayer, and F. J. Litterst, Phys. Rev. Lett. **91**, 017204 (2003).
[15] A. Suter, E. Morenzoni, R. Khasanov, H. Luetkens, T. Prokscha, and N. Garifianov, Phys. Rev. Lett. **92**, 087001 (2004).
[16] P. G. de Gennes, *Superconductivity of Metals and Alloys* (Addison-Wesley, New York, 1989).
[17] S. H. Brongersma, E. Verweij, N. J. Koeman, D. G. de Groot, R. Griessen, and B. I. Ivlev, Phys. Rev. Lett. **71**, 2319 (1993).
[18] A. K. Geim, S. V. Dubonos, I. V. Grigorieva, K. S. Novoselov, F. M. Peeters, and V. A. Schweigert, Nature (London) **407**, 55 (2000).
[19] J. Guimpel, L. Civale, F. de la Cruz, J. M. Murduck, and I. K. Schuller, Phys. Rev. B **38**, 2342 (1988).
[20] G. P. Felcher, R. T. Kampwirth, K. E. Gray, and R. Felici, Phys. Rev. Lett. **52**, 1539 (1984).
[21] M. P. Nutley, A. T. Boothroyd, C. R. Staddon, D. M. Paul, and J. Penfold, Phys. Rev. B **49**, 15789 (1994).
[22] H. Zhang, J. W. Lynn, C. F. Majkrzak, S. K. Satija, J. H. Kang, and X. D. Wu, Phys. Rev. B **52**, 10395 (1995).
[23] S. W. Han, J. F. Ankner, H. Kaiser, P. F. Miceli, E. Paraoanu, and L. H. Greene, Phys. Rev. B **59**, 14692 (1999).
[24] C. Bolech, G. C. Buscaglia, and A. Lopez, Phys. Rev. B **52**, R15719 (1995).
[25] S. J. Blundell and J. A. C. Bland, Phys. Rev. B **46**, 3391 (1992).
[26] U. Pietsch, V. Holy, and T. Baumbach, *High-Resolution X-Ray Scattering* (Springer, New York, 2004).
[27] H. Frahm, S. Ullah, and A. T. Dorsey, Phys. Rev. Lett. **66**, 3067 (1991).
[28] F. Liu, M. Mondello, and N. Goldenfeld, Phys. Rev. Lett. **66**, 3071 (1991).
[29] R. Kato, Y. Enomoto, and S. Maekawa, Phys. Rev. B **47**, 8016 (1993).
[30] M. Machida and H. Kaburaki, Phys. Rev. Lett. **71**, 3206 (1993).
[31] M. Tinkham, *Introduction to Superconductivity*, 2nd ed. (Dover, New York, 2004).
[32] C. S. L. Chun, G.-G. Zheng, J. L. Vicent, and I. K. Schuller, Phys. Rev. B **29**, 4915 (1984).